ANALYSIS OF ASCAT, SMOS, IN-SITU AND LAND MODEL SOIL MOISTURE AS A REGIONALIZED VARIABLE OVER EUROPE AND NORTH AFRICA

Nazzareno Pierdicca[a], Fabio Fascetti[a], Luca Pulvirenti[b,a], Raffaele Crapolicchio[c,d], Joaquin Muñoz-Sabater[e]

[a] *Department of Electronic Engineering, Sapienza University of Rome. Via Eudossiana 18 - 00184 Rome, Italy*

[b] *CIMA Research Foundation, Via A. Magliotto 2 - 1700 Savona, Italy*

[c] *Serco SpA. Via Sciadonna 24/26 - 00044 Frascati, Roma, Italy*

[d] *ESA-ESRIN. Via Galileo Galilei, Casella Postale, 00044 Frascati, Roma, Italy*

[e] *European Centre for Medium-Range Weather Forecasts (ECMWF), Reading, UK*

ABSTRACT

A comparison of soil moisture products derived from satellite data, in-situ measurements and land models was performed in the frame of the EUMETSAT H-SAF project. In particular, soil moisture retrievals of ASCAT/H-SAF and SMOS were compared with two other independent datasets, that are the NCEP/NCAR volumetric soil moisture content reanalysis developed by NOAA, and the ERA-Interim/Land soil moisture produced by ECMWF. In situ data available through the International Soil Moisture Network and distributed in regions comprising Denmark, France, Germany, Italy, Poland and Spain, were also included in the comparison. The whole H-SAF region of interest, including Europe and North Africa, was considered and the period between January 2010 and December 2012 was analysed.

The Triple Collocation (TC) approach was adopted to perform the comparison exercise. TC was critically reviewed to compare different solutions proposed in the literature and to discuss the possibility of performing a point-wise TC, or a *global* TC, which considers each system as a whole, with unique gains and error standard deviations in the whole area. The TC results showed a very good behaviour of the ERA land model, while SMOS satellite slightly outperformed ASCAT or vice versa, depending on factors like the geographical area or the consideration of the whole dynamic range of soil moisture or only the anomalies with respect to the seasonal variability.

Keywords: soil moisture, triple colocation, H-SAF, ASCAT, SMOS

1. Introduction

Soil moisture represents a key variable for the characterization of the global climate, since it influences the water cycle by controlling the partition of rainfall between land (infiltration, percolation and runoff) and the atmosphere (evaporation and plant transpiration). Its knowledge is essential for several applications, such as drought and flood prediction, weather forecast, climatology and agronomy. Soil moisture maps from satellite are currently assimilated within hydrological models (e.g. Brocca et al., 2012), or used as realistic initial states by numerical weather prediction (NWP) models (e.g. Panegrossi et al., 2011).

Microwave remote sensing is a very useful tool to monitor soil moisture at different spatial and temporal scales, with spatial resolution ranging from tens of kilometres for wind scatterometers and microwave radiometers, to the order of meters for Synthetic Aperture Radar (SAR) systems, although the latter have poorer temporal and radiometric resolutions. The first spaceborne mission carrying a microwave radiometer designed for this application, i.e., the European Space Agency (ESA) Soil Moisture and Ocean Salinity (SMOS) satellite (Kerr et al., 2001), launched in November 2009, uses a L-band (~1.4 GHz) interferometric radiometer (MIRAS) to retrieve soil moisture content (*SMC*). At present, no data from active L-band instruments are available since ALOS-2 (launched on May 24, 2014) is still in its commissioning phase and the launch of the Soil Moisture Active Passive (SMAP) mission by NASA (carrying aboard both a L-band radiometer and a L-band radar, see Brown et al., 2013) is foreseen in early 2015.

Even sensors operating at higher frequency, such as C-band, turned out to be useful for *SMC* retrieval. In particular, sensitivity to *SMC* was demonstrated by the Advanced Microwave Scanning Radiometer - Earth Observing System (AMSR-E) aboard the AQUA satellite (e.g. Gruhier et al., 2010) and by active instruments, such as the scatterometer aboard the European Remote Sensing (ERS) satellites and the Meteorological Operational (MetOp) satellite operated by the European Organization for the Exploitation of Meteorological Satellites (EUMETSAT) (e.g. Wagner et al., 1999, Bartalis et al., 2007). C-band SAR data were used to produce high spatial resolution *SMC* maps by relying on proper retrieval techniques, such as change detection (Hornáček et al., 2012), multitemporal methods (Pierdicca et al., 2010; Pierdicca et al., 2013, Mattia et al., 2013), artificial neural networks (Paloscia et al., 2013), as well as by taking advantage of polarimetric measurements (e.g. Pierdicca et al., 2008).

The EUMETSAT Satellite Application Facility (SAF) on Support to Operational Hydrology and Water Management (H-SAF) was established by EUMETSAT council in July 2005. The objective is the provision of new satellite-derived products for use in operational hydrology. Within the framework of the H-SAF project, the validation of the soil moisture products, derived from the C-band data of the Advanced SCATeremoter (ASCAT) on board MetOp, is presently accomplished. Different institutions in Europe are involved in the validation task, coordinated by the Italian Department of Civil Protection. A possible validation strategy consists in assessing the ASCAT-derived *SMC* product through a comparison with retrievals from an instrument explicitly designed to measure soil moisture, such as SMOS, as well as with ground networks or outputs of hydrological Land Surface Models (LSM).

Many different studies can be found in the literature comparing different satellite-derived soil moisture datasets in different places. For instance, Parrens et al. (2012) found consistent values between SMOS and ASCAT, especially in wet conditions, with the latter outperforming the former in some situations. Albergel et al. (2012) added to this comparison outputs from the ECMWF land surface model, concluding that SMOS performances exhibit a weaker dependence on seasons with respect to ASCAT. ASCAT, SMOS and AMSR-E retrievals were compared by Leroux et al. (2013), whereas Rüdiger et al. (2009) assessed AMSR-E and the ERS scatterometer, and Brocca et al. (2011) the ASCAT and AMSR-E products. When compared to in-situ data, some differences were noticed, as a consequence of factors such as geographical area or type of land cover, but no definitive conclusions emerged on what sensor outperforms the others.

When comparing measurements from different sensors or models, it is necessary to assume one of them as the reference, i.e., the one which provides the “truth”. However, this assumption may be questioned since errors generally affect satellite retrievals, physical models and even ground data. Consequently, the Triple Colocation (TC) approach is often adopted. It is a statistical method that can be used for estimating the relative error variance of three datasets with independent error structures (Stofflen, 1998; Scipal et al., 2008). To compare datasets with different spatial sampling and amplitude scales, previous works collocated the retrievals to a regular grid using a nearest neighbour resampling and standardize the data in different ways. One consists of making standard deviation (σ) and seasonal mean (μ) equal to those of the product taken as reference (Anderson et al., 2010). This is a critical aspect of the comparison which should be taken with care, as adjusting σ and μ in each point of the *SMC* map is not providing an assessment of a satellite platform as a unique probing system characterised by its own bias and gain. Besides the comparison of absolute values of soil moisture, the anomaly values (i.e., with respect to the seasonal trend) can be used to gather information about the capability of the different products to detect single events of wetting and drying (Parinussa et al., 2011).

In Dorigo et al. (2010), the error characterization was carried out, using the TC technique applied to the anomalies, to reveal trends in uncertainty between active (ASCAT) and passive soil moisture products derived from different AMSR-E channels. The anomalies of SMOS, ASCAT and AMSR-E Land Parameter Retrieval Model (LPRM) products were analysed by Leroux et al. (2011) during year 2010, concluding that SMOS reported the best overall results over the USA.

This paper presents an extensive comparison of soil moisture products derived from ASCAT/H-SAF and SMOS satellite data, in-situ measurements available throughout the International Soil Moisture Network (ISMN) and LSM predictions, namely the NCEP/NCAR volumetric soil moisture content reanalysis, developed by the National Oceanic and Atmospheric Administration (NOAA) and the ERA-Interim/Land soil moisture produced by ECMWF. The exercise was performed in the frame of the EUMETSAT H-SAF project by carrying out a TC analysis; note that in the literature slightly different solutions to the problem of retrieving the error variance of three sources of *SMC* data can be found and the same applies for the methods to normalize the data. Hence, we reconsidered the TC mathematical background taking into account that soil moisture is a random function of space and time, which is not stationary. This novel approach allows a *global* TC be performed, characterizing satellites and models by a unique error variance. The whole H-SAF region of interest, including Europe and North Africa, was considered and the period between January 2010 and December 2012 was analysed. This 3-year period, which includes several seasonal cycles, overpasses many previous analyses, thus representing a significant time and spatial extent. Note that in most of the literature papers, shorter intervals and/or smaller areas (e.g., one country) were considered, with the exception of few studies working at global scale, such as Dorigo et al. (2010).

An overall description of the diverse data sets used in this study is provided in section 2, which depicts also the methodology (data aggregation, resampling, quality control) used to compare the different data sets. Section 3 is devoted to a review of the TC technique and a discussion on alternative approaches found in the literature. The results of the TC analysis are discussed in section 4 and the conclusions of this paper are summarized in section 5.

2. Data sets and pre-processing steps

2.1 Available data sets

Hereafter only a short description of the considered data sets and their most relevant features is reported; more details can be easily found in the literature (e.g., Albergel et al., 2012).

2.1.1 In-situ soil moisture

The International Soil Moisture Network (ISMN, see http://ismn.geo.tuwien.ac.at) is an international cooperation coordinated by the Global Energy and Water Exchanges Project

(GEWEX) in collaboration with the Group of Earth Observation (GEO) and the Committee on Earth Observation Satellites (CEOS), with the task of maintaining a global in-situ soil moisture database. The data collected by many different probe networks around the world are useful for validating and improving global satellite observations and land surface models. The ISMN includes ancillary information, such as soil temperature, precipitation and air temperature (Dorigo et al., 2011). For our study, the data collected at 0-5 cm depth in Denmark, France, Germany, Italy, Poland and Spain (with average number of stations 30, 20, 15, 1, 2 and 20, respectively) were used throughout the period from 2010 to 2013.

2.1.2 SMOS L2 soil moisture

The payload on-board the SMOS satellite is the MIRAS instrument; it is an interferometric radiometer that measures the cross correlation between pairs of receivers to derive a visibility function (Kerr et al., 2001; Kerr et al., 2012). Brightness temperatures are measured at several incidence angles (from 0° to 65°), sensing the horizontal and vertical polarizations, and also the 3rd and 4th Stokes parameters. MIRAS operates at 1.427 GHz (L-band) from an orbit of 758 km, with a repetition time of 3 days and a horizontal spatial resolution between 35 and 50 km.

The reprocessed ESA L2 product, that provides an actual volumetric moisture content (*SMC*, in m^3/m^3), was considered in this work; L2 data are sampled over the ISEA4h9 grid, which has a spacing in the order of 15 km (Kidd, 2005). It is important to underline that the processor generating the products is the 5.51 version; in fact, in March 2012 the SMOS processing chain was modified, including a different model of soil permittivity with respect to that used within the previous 5.01 version.

2.1.3 ASCAT soil moisture index

ASCAT is a radar instrument that operates at C-band in vertical polarization and measures the backscatter coefficient (Bartalis et al., 2007). Measurements are taken on both sides of the sub-satellite track over two 550 km wide swaths, from a 817 km height orbit, resulting in a global coverage achieved in about 1.5 days over Europe. The “large scale surface soil moisture” product, that is available through the EUMETSAT H-SAF project, was used for the comparison (hereafter denoted as H07 SM-OBS-1, according to the H-SAF nomenclature in http://hsaf.meteoam.it/index.php). The data are sampled on a 25 km grid and the product is generated by means of an algorithm originally conceived for the ERS-1/2 scatterometer, by the Technical University of Wien (Wagner et al., 1999) and successively updated (Naeimi et al., 2009). The algorithm is based on a change detection approach which assumes that soil moisture is linearly related to backscattering (in dB units) and that the temporal changes of surface roughness, canopy structure and vegetation biomass occur at longer temporal scales than soil moisture changes, so that moisture variation in time can be detected. For each SM-OBS-1 map, a pixel value represents a relative value, i.e., an index between 0% and 100%, with respect to the driest and the wettest conditions registered for that pixel during the calibration phase of the algorithm. Assuming that these conditions represent completely dry and wet soils, respectively, this index is equal to the saturation degree (*SD*), i.e., the soil moisture content expressed in percent of porosity.

2.1.4 Soil moisture reanalysis

The NCEP/NCAR reanalysis volumetric soil moisture content, available from the NOAA website (http://www.ngdc.noaa.gov/), was used as independent source to assess the satellite products. These data represent a daily analysis/estimate of the volumetric soil moisture within a depth between 0 and 10 cm, available four times a day at 00:00, 06:00, 12:00 and 18:00 UTC, and sampled over a T62 Gaussian grid with 192×94 points (about 2×2 degrees spacing). Another dataset used in this work is the ERA-Interim/Land produced by ECMWF, hereafter denoted as ERA-LAND. It is a global atmospheric reanalysis combined with an ocean and a land surface model available until 2012. Soil moisture is provided at four different layers and four time steps (at 00:00, 06:00, 12:00 and 18:00 UTC) each day over a grid with a space sampling of 0.125×0.125 degrees (Balsamo et al., 2014).

The two different LSM-derived *SMC* have very different characteristics (very coarse vs medium spatial resolution, different parameterizations for surface processes), which actually influence the results, so that it is worth to use both of them in our comparison exercise, and shortly resume some differences and similarities.

2.1.5 Soil porosity

The soil porosity map available from the Global Land Data Assimilation System (GLDAS) website (http://ldas.gsfc.nasa.gov/gldas/) and based on the Food And Agriculture (FAO) Soil Map of the World was used to convert *SD* into absolute *SMC*. The map is resampled at 1/4 and 1 degree horizontal resolution and three possible depths; the top porosity (0-2 cm) was used for our purposes.

2.2 ASCAT rescaling

A critical aspect of the comparison is the different units in which satellite products are expressed, that are the ASCAT relative *SD* (denoted by SD_{ASCAT}), in the range 0-100, and the SMOS absolute *SMC* (denoted as SMC_{SMOS}), in m^3/m^3 (or % m^3/m^3 when multiplied by 100). Before comparing the two products, a common practice is performing a point-wise standardization of the mean and the standard deviation of the collocated products, as well as a matching of their respective histograms.

Here SD_{ASCAT} was converted into a volumetric moisture in m^3/m^3 considering that, by definition, it represents the distance of each resolution cell from its driest and wettest soil conditions. For this purpose, maps of the maximum and minimum *SMC* values, denoted as min(*SMC*) and max(*SMC*), were computed using different datasets. Firstly, they were estimated from SMOS L2 data; to avoid outliers slipped in the computed maps, the first and last percentiles were disregarded. Additionally, and in order to have reliable estimates of extreme values, these maps were computed using all SMOS available retrievals (i.e., not only those collocated with ASCAT), retaining only grid points with significant statistics (i.e., number of total observations greater than 50, with a minimum number of 6 observations in Summer, Spring and Autumn). Alternatively, min(*SMC*) and max(*SMC*) were derived in the same way from other independent sources, namely the ERA-LAND and NOAA data collected throughout the period 1990-2012 (a timeframe comparable to the period of calibration of the ASCAT retrieval algorithm). Then, for each SMOS grid point, the collocated SD_{ASCAT} was converted into an absolute SMC_{ASCAT} through the following linear transformation, which assigns min(*SMC*) and max(*SMC*) to the driest (SD_{ASCAT}=0) and wettest (SD_{ASCAT}=100) conditions:

$$\frac{SMC_{ASCAT} - \min(SMC)}{\max(SMC) - \min(SMC)} = \frac{SD_{ASCAT}}{100} \qquad (1)$$

In **Figure 1**, the maps of min(*SMC*) and max(*SMC*) (see section 2.2) generated to rescale ASCAT are presented, along with the mean *SMC*.

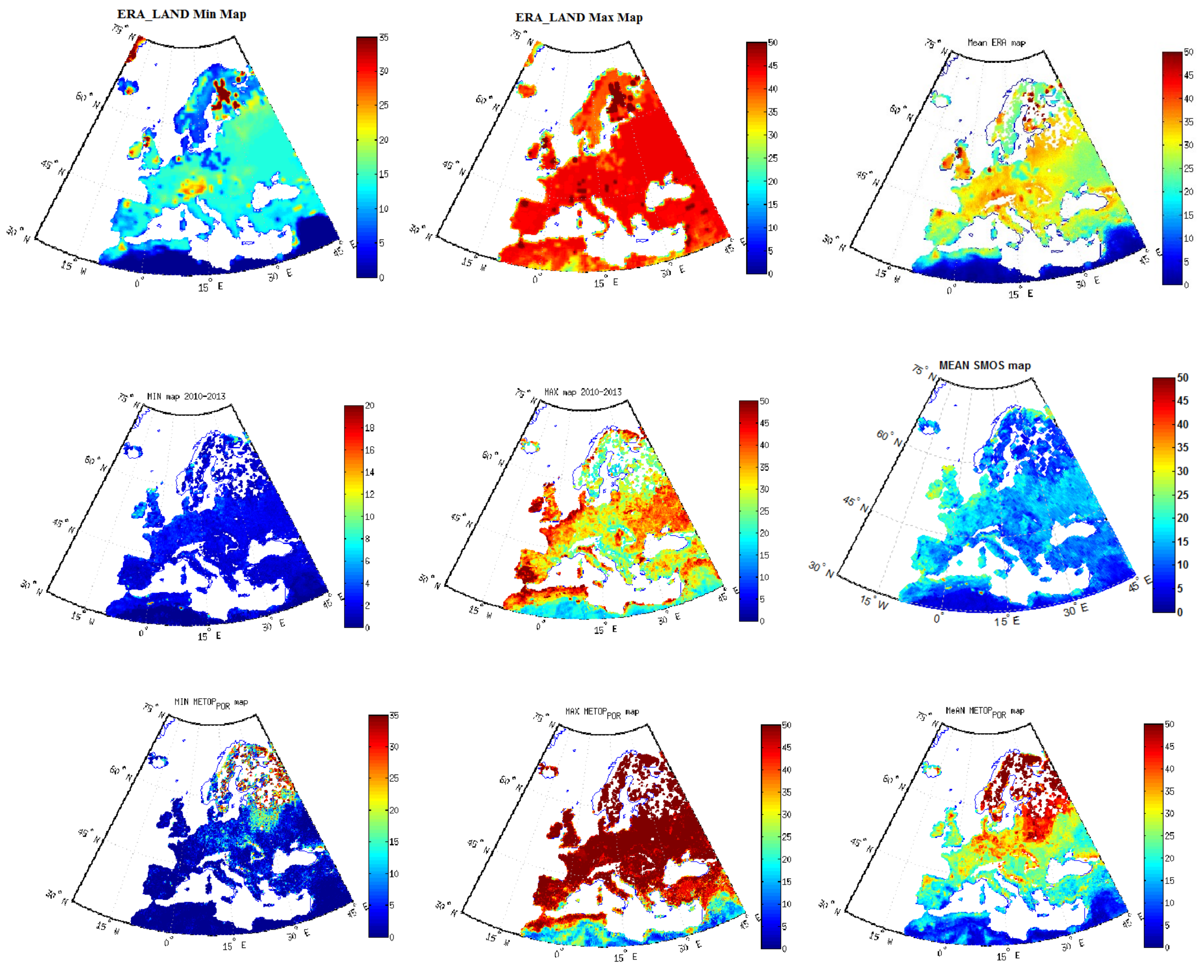

Figure 1: Maps of minimum (left), maximum (central) and mean (right) values of *SMC* derived from ERA (upper row, years 1991-2012), SMOS with processor version 5.51 (middle row, years 2010-2013) and ASCAT product rescaled using the porosity map (bottom row, years 2010-2013).

Finally, taking advantage of the availability of a soil porosity (ϕ) map, SD_{ASCAT} was transformed into SMC also by multiplying it by ϕ, i.e., $SMC_{ASCAT} = \phi\, SD_{ASCAT}/100$. In the following analysis (section 4) it will be specified what scaling method is used to transform SD_{ASCAT} into SMC_{ASCAT}.

2.3 Data colocation

2.3.1 Colocation of satellite estimates and LSM data

SMOS, ASCAT, LSM-derived *SMC*, and the porosity map were resampled over the same ISEA4h9 grid. As a first step, ASCAT and SMOS data were co-located in time and space, retaining only data fulfilling the following conditions: *i*) SMOS retrievals with Data Quality Index (DQX) less than 0.045 ; *ii*) ASCAT retrievals with less than 4 processing flags up (see H-SAF Product User Manual at http://hsaf.meteoam.it/) ; *iii*) SD_{ASCAT} with value between 0 and 100% (values outside this range can be found and were assumed as unreliable); *iv*) SMOS and scaled ASCAT *SMC* retrievals below 0.7 m^3/m^3 (as greater values are not plausible).

For each SMOS grid point, the closest ASCAT gridded observation was searched using the nearest neighbour approach. To minimize the temporal mismatch between ASCAT and SMOS observations, ascending MetOp orbits and descending SMOS orbits (around 21:30 and 18:00 local time, respectively) and vice versa (at 9:30 and 6:00) were combined. This approach led to a data set with the most probable value of the spatial mismatch equal to 6.5 km, with maximum of 9 km, and in the order of 200 minutes for the temporal mismatch.

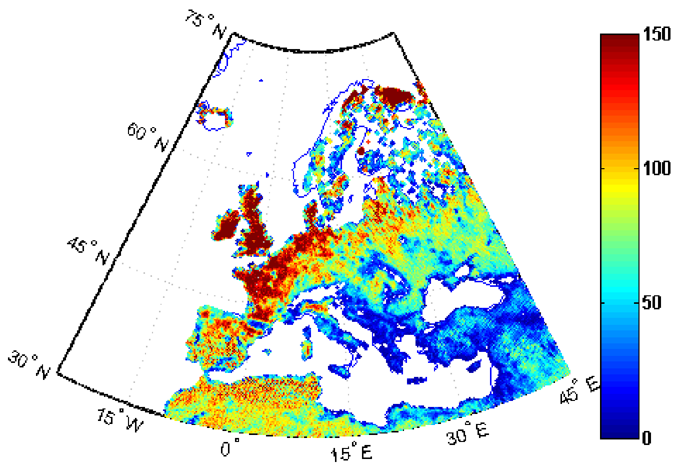

Figure 2: Number of colocations of SMOS, ASCAT/H-SAF and ERA-LAND estimates in each point of the ISEA4h9 in the considered time frame grid (January 2010 – December 2012). Note that grid points with more than 150 occurrences are about 4% of the total.

The nearest neighbour approach was adopted to resample ERA-LAND, NOAA and the porosity information on the ISEA4h9 grid. A maximum distance of 9 km from the ISEA4h9 grid was considered for ERA-LAND, with resulting most probable distance of 5.5. km, whereas in the case of the low resolution NOAA data, the most probable distance turned out to be 60 km.

An overall picture of the quantity of collocated data is shown in **Figure 2**, where in each ISEA4h9 grid point the number of triple colocations (SMOS, ASCAT and ERA-LAND) is represented. Note that the colocations were basically determined by the SMOS and the ASCAT/H-SAF products, and constrained mainly by orbits and to some extent by the occurrence of Radio Frequency Interference (RFI) or poor quality indices, whereas including the model outputs from ERA-LAND does not diminishes significantly (less than 2.4%) the number of colocations.

2.3.2 Colocation of satellite estimates and in situ data

As for the colocation with the ISMN data, all the stations probing *SMC* at 0-5 cm depth were analysed and the probes with anomalous behaviour were filtered out by visual inspection of their temporal plots. Subsequently, the measurements were up-scaled to the satellite resolution, through averaging of the in-situ measurements within the satellite field of view. Specifically, for each satellite's gridded product, the gauges within a radius distance of 22.5 km for SMOS (distance from the ISEA4h9 grid points), which is the mean of the Antenna FootPrint (AFP) parameter, and of 25 km for ASCAT (distance from the latitude and longitude annotated in the product) were considered. Moreover, only satellite values with at least one station closer than 10 km were retained in order to gather in situ measurements sufficiently representative of the satellite field of view. **Figure 3** depicts how the ISMN data were associated to satellite data, showing that it was possible to have different stations associated to SMOS (blue and yellow in the figure) and ASCAT (blue and red) observations and sampled at different times.

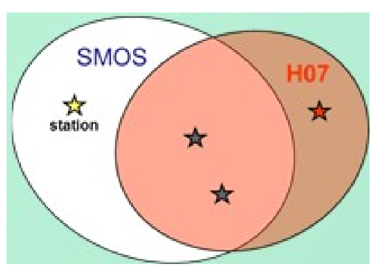

Figure 3: Example of ISMN data up-scaling approach. Blue stars are stations associated to both ASCAT and SMOS field of view, the yellow star is associated only to SMOS and the red star only to ASCAT.

3. The triple colocation: review and adopted approach

3.1 Triple colocation summary

In order to validate any satellite product one should have a reference data set to be considered as the “true”. Since any reference has its own error, which is unknown and then would affect the validation results, the Triple Colocation (TC) analysis combines three data sources and estimate their relative errors without any prior assumption on their magnitude. It was originally introduced for validating ocean wind scatterometer products by Stoeffelen (1998) and Freilich and Vanhoff (1999, 2001), successively by Caires and Sterl (2003), and later applied to the validation of global soil moisture estimates (Scipal et al., 2008; Miralles et al., 2010; Dorigo et al., 2010). Here we adopt the formalism introduced by Stoeffelen (1998), with some extensions to account for later works. In the following the procedure is briefly reviewed, with the main scope of highlighting some differences among the solutions adopted in the literature which, to our knowledge, were not pointed out in previous papers.

Suppose that three measurement systems *X*, *Y*, and *Z* are measuring a true variable θ (*SMC* in this case). Let us assume the following model error for measurements *x*, *y*, *z* provided by the three systems:

$$
\begin{aligned}
x &= s_x(\theta + b_x + \delta x) \\
y &= s_y(\theta + b_y + \delta y) \\
z &= s_z(\theta + b_z + \delta z)
\end{aligned}
\qquad (2)
$$

where δx, δy and δz represent the random observation errors with zero mean, i.e., $\langle \delta_x \rangle = \langle \delta_y \rangle = \langle \delta_z \rangle = 0$, and variance $\epsilon_x^2 = \langle \delta_x^2 \rangle$, $\epsilon_y^2 = \langle \delta_y^2 \rangle$, $\epsilon_z^2 = \langle \delta_z^2 \rangle$, while s_x, s_y and s_z are scaling factors, or gains of the systems supposed to have a linear response, and b_x, b_y

and b_z account for mean errors different from zero. Note that since the X system is assumed as the reference s_x=1 and b_x=0 even if not clearly stated (Dorigo et al., 2010). Then, although the bias terms (b_x, b_y and b_z) were ignored by Stoeffelen (1998), the solution still applies as shown in the sequel. The true variable is considered varying randomly, with variance denoted as $\sigma^2 = \langle(\theta - \langle\theta\rangle)^2\rangle$, being its mean value in our paper not necessarily zero, as opposed to what was assumed by Stoeffelen (1998).

Usually, the three systems do not represent the same spatial scale of the observed field θ (*SMC* in our case), and thus it is assumed that X and Y can resolve smaller scales than that resolved by Z. Hence the variance common to the smaller scales, i.e., $\sigma_r^2 = r^2$ is introduced; it represents, by definition, the correlated part of the representativeness errors of X and Y. In other words, θ refers to the large scale features of the observed field, which is measured by Z, whereas the small scale features sensed by X and Y are embedded in the noise terms δ_x and δ_y.

Except for the representativeness error, it is assumed that the errors of the different observation systems are not correlated, i.e. $\langle\delta_x \delta_z\rangle = \langle\delta_y \delta_z\rangle = 0$, and also not correlated with the true random variable, i.e., $\langle\theta \delta_x\rangle = \langle\theta \delta_z\rangle = \langle\theta \delta_y\rangle = 0$. Conversely, because of the representativeness error, it is assumed $\langle\delta_x\delta_y\rangle = r^2$. With the above assumptions it is possible to derive the unknown error structure by computing some statistical moments of the collocated database as demonstrated in the Appendix. Starting from eq. (A.2) and introducing the correlation coefficients among observations, i.e., ρ_{xy}, ρ_{xy}, and ρ_{xy}, the variance of the random errors affecting the three systems can be expressed as:

$$\varepsilon_x^2 = \sigma_x^2\left[1-\rho_{xy}\rho_{xz}/\rho_{yz}\right]+\sigma_r^2$$

$$\varepsilon_y^2 = \sigma_x^2\left[\rho_{xz}^2/\rho_{yz}^2-\rho_{xy}\rho_{xz}/\rho_{yz}\right]+\sigma_r^2$$

$$\varepsilon_z^2 = \sigma_x^2\left[\left(\rho_{xy}/\rho_{yz}-\sigma_r^2/\sigma_x^2\rho_{xz}\right)^2-\rho_{xy}\rho_{xz}/\rho_{yz}\right]+\sigma_r^2 \quad (3)$$

In the literature, different formalisms to implement the TC approach can be found, although the hypotheses are basically the same. They differ in that they may or may not assume the presence of bias terms, and account for the correlated component of the representativeness error. A difference solution of the system in (2) is proposed in some works, as Dorigo et al. (2010) and Scipal et al. (2008). Following a mathematical development reported in the Appendix and leading to eq. (A.4), substituting eq. (A.3) and extracting the common factor σ_x^2, the variance of the errors becomes expressed by:

$$\varepsilon_x^2=\sigma_x^2\left[1-\rho_{xy}-\rho_{xz}+\rho_{yz}\right]$$

$$\varepsilon_y^2=\sigma_x^2\left[1-\rho_{xy}+\rho_{xz}-\rho_{yz}\right] \quad (4)$$

$$\varepsilon_z^2=\sigma_x^2\left[1+\rho_{xy}-\rho_{xz}-\rho_{yz}\right]$$

It is interesting to note that the latter solution is different from (3), not only for the absence of the representative error, but also for the additive structure of the correlation terms, as compared to the multiplicative structure of (3). In both cases, for instance, the errors of the three systems are considered zero if the correlation coefficients are all equal to one, so that no errors are actually expected. In the case that the correlation coefficients tend to zero, both solutions infer that the system error variances equal the measurement variances. As for other conditions, the difference between the two solutions can be relevant. For instance, if x is uncorrelated to y and z (thus σ_r^2=0), which on their turn are perfectly correlated, from (3) it comes out that system X has error covariance equal to the measurement covariance, whilst systems Y and Z are not affected by errors at all. Conversely, (4) predicts an error covariance of system X two times the measurement covariance. The difference comes up since eq. (A.1) is actually estimating the gain terms in the 3-dimensional space, whereas according to eq. (A.3) they are estimated independently in each plane referring to a pair of measurements. In the sequel we will adopt the solution represented by (3) based on the correlation coefficients.

3.2 Regionalised random functions

In section 3.1 constant values of the true variable mean and variance were assumed. However, soil moisture is actually a random function (RF) of time and space, and its seasonal variabilities in a given site, or the large scale spatial variabilities related to meteorological and surface properties at different sites, have to be considered. These variabilities can be considered random or deterministic, and the true variable can be considered as a space-temporal RF of space **r** and time t, with first and second order statistics constant only in case of a stationary RF.

Here the true soil moisture is assumed as a second order intrinsic stationary RF with zero mean plus a space-time drift. It is supposed that space and time dependent functions additively combine to form the drift $m(\mathbf{r},t)$:

$$\theta'(r,t)=\theta(r,t)+m(r,t)=\theta(r,t)+m_r(r)+m_t(t) \tag{5}$$

Since in (2) θ is considered a RF with same mean value whatever place and time, the drift must be removed. To this aim, $m_r(\mathbf{r})$ is estimated by averaging the *SMC* maps over time, while $m_t(t)$ is evaluated by fitting the spatial mean versus time by an harmonic function with period of 365 days, i.e., $a_i \cdot \cos(2\pi t/365+\varphi_i)$, where amplitude a_i and phase φ_i are independently estimated for the three systems, that is i=x,y,z. In this case the TC analysis is performed on the residuals, or anomalies, with respect to the mean spatial pattern and seasonal variability, as done in many works. Note that in other works (i.e., Parinussa et al., 2011; Miralles, et al., 2011) the temporal trend was estimated by an averaging moving window (generally 30 days long). This is not a reliable solution if the time sampling of each grid point is not regular and frequent enough due to the difficulty of finding collocated satellite data (see **Figure 2**). In our case we got 1031 samples of the spatial means in a timeframe of 3 years. They are very noisy since the daily coverage of the colocation is poor, but in any case enough to register the seasonal oscillation, so that fitting the temporal trend with a sinusoidal function seems to be a suitable method. A visual check of data and fitting curve as function of time (not reported for conciseness) confirmed the better performances of the harmonic fitting.

As mentioned before, the drift can be considered as part of the random variability, but this is feasible only for the temporal drift, thanks to the fact that our data set encompasses a time frame much larger (3 years) than the annual period of the seasonal drift. In other words, we are capable to sample even the lower frequencies of the temporal variability and thus to estimate the variance and covariance of $\theta(\mathbf{r},t)+m_t(\mathbf{r},t)$, assumed as a stationary RF. This is not the case for the spatial drift, as our data set does not extend to the whole globe and the variance and covariances would in this case depend on the dimension of the considered area. In the sequel we will consider two cases: i) removing only the spatial drift from the original observations (i.e., retaining the seasonal trend); ii) removing both spatial and temporal drifts (i.e., looking only at the anomalies).

4. Triple colocation results

The TC was firstly applied point wise to the satellite products and the LSM outputs, independently for each grid point of the collocated maps. In this way we are analysing the capability to reproduce the temporal variability, assuming that in each point the gain and bias parameters of each measurement system in respect to the reference can be different. This is a usual practice found in the literature dealing with soil moisture or rain rate retrievals (i.e., Dorigo et al., 2010). However, when dealing with satellite systems and models, as in this work, it can be expected that bias and gain are not site-dependent, so that a *global* TC was also performed to characterize each system as a whole, as explained in section 3.2. Then, the TC analysis was carried out considering the in-situ data instead of the LSM outputs, although in this case only the *global* TC characterization was feasible, as the number of observations collocated to the satellite soil moisture in one site was not sufficient to lead to significant error estimates.

4.1 Triple colocation of SMOS, ASCAT and LSM outputs

A TC analysis using data from SMOS, ASCAT/H-SAF and ERA-LAND collocated on the ISEA4h9 grid was performed. The NOAA model instead of ERA-LAND was also considered, although the latter was expected to provide better results, at least for its finer spatial resolution.

4.1.1 "Point-by-point" triple colocation analysis

The total number of colocations is 4,279,434 out of the 59,116 grid points, with spatial distributions shown in **Figure 2**. The results of the analysis without removing the temporal trend are presented in **Figure 4**, where the differences are a direct consequence, according to (4), of the temporal correlations. Note that any linear normalization does not affect the correlation coefficient in each grid point (i.e., the temporal correlation coefficient), so that in a "point-by-point" TC the scaling of ASCAT is ineffective and the original *SD* product can be considered as well.

Overall, the range of error standard deviation of the three sources, expressed as mean and standard deviation of ε_x, ε_y, ε_z in the considered area, is 3.04±2.04% m^3/m^3, 3.54±2.47% m^3/m^3 and 3.75±2.82% m^3/m^3, for ERA, ASCAT/H-SAF and SMOS, respectively. In this statistics we discarded error estimates outside the range [0%-100%], i.e., only 65% of the ISEA4h9 grid points were retained (quite randomly distributed in the area of interest). Note that the gains are also different for the three sources; in particular SMOS has a dynamic range generally smaller than ERA (i.e., the reference), whereas the dynamic range of ASCAT/H-SAF *SD* is larger because, according to its different definition, it ranges from 0 to 100%.

In **Figure 4** (upper row) it can be observed that SMOS provides in general the worst performances, due to the lower temporal correlation with ASCAT/H-SAF and ERA-LAND, while the correlation between the latter two datasets is higher. In fact, the temporal correlations between different datasets were computed in each point of the ISEA4h9 grid (maps are not shown for conciseness) finding out that the temporal correlation between ASCAT and ERA is high in most of the Central Europe, while lower values were obtained considering SMOS and ERA. Actually, there are areas where the situation is the opposite, like for example the desert, where ASCAT/H-SAF exhibits negative correlation with respect to both SMOS and ERA-LAND which, on their turn, have a positive temporal correlation in this geographical area. Note that according to this point wise analysis, the ASCAT/H-SAF error standard deviation is still low over desert (**Figure 4**, upper central panel), thus the ASCAT/H-SAF failure is revealed only by noticing in the lower left panel of **Figure 4** the negative value of the scaling factor over most of the grid points in this area. This is an example of the limitation of the point wise TC analysis.

For a better comparison among systems, **Figure 5** shows, through an RGB level slicing (red, green and blue points indicates ERA-LAND, ASCAT/H-SAF, and SMOS, respectively), where each system performs worse (left panel) or better (right panel) than the others. Close to the Mediterranean coast of Spain there are zones where SMOS presents the best behaviour, but it generally gives the worst performances in most of the Central European countries. Surprisingly, ERA-LAND performs better than the other systems in a large portion of the investigated area, while ASCAT/H-SAF exhibits the least error in the Northernmost and Easternmost areas, with worse performances over the desert and most arid areas.

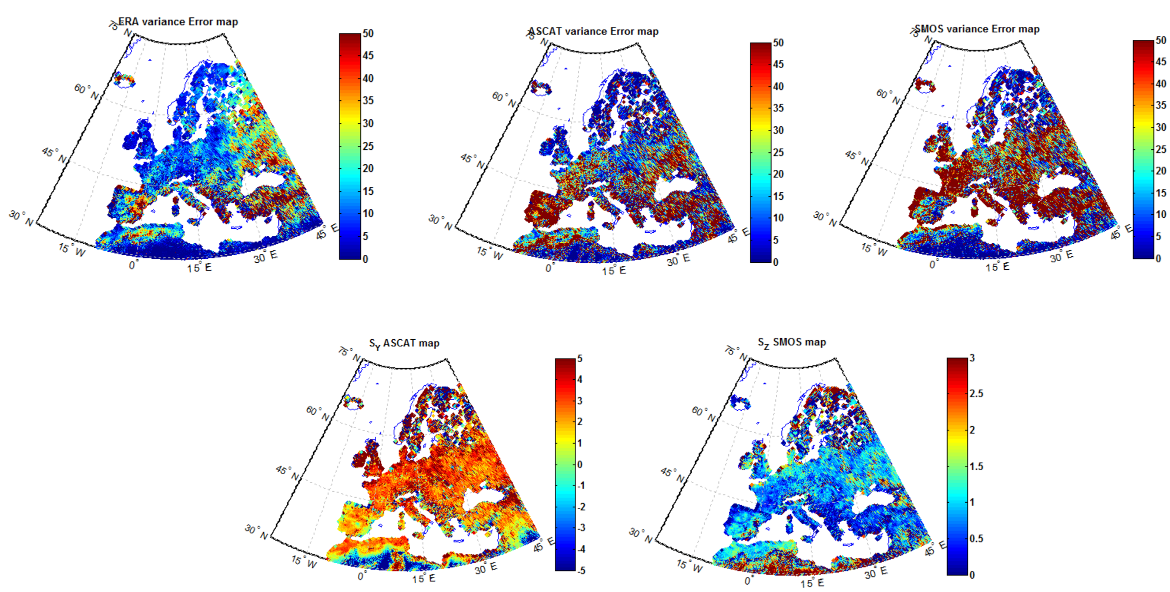

Figure 4: Point wise TC analysis results. Upper row: error variances of ERA-LAND (left panel), ASCAT/H-SAF *SD* (middle panel) and SMOS *SMC* (right panel) systems, all reported in the scale of the ERA-LAND product taken as reference. Bottom row: gain of ASCAT/H-SAF *SD* (left panel) and SMOS (right panel).

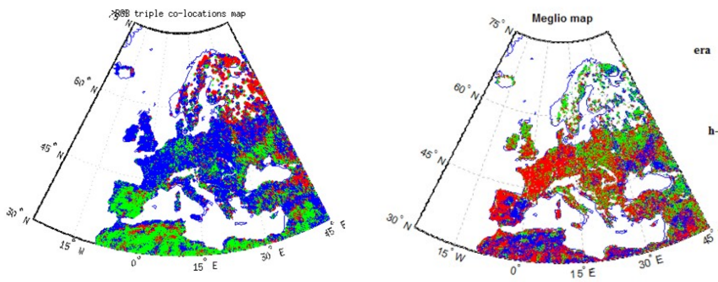

Figure 5: RGB level slicing depicting what system performs worse (left) and better (right) than the others. Red: ERA-LAND; green: ASCAT/H-SAF; blue: SMOS**.**

4.1.2 "Global" triple colocation analysis

When considering the three systems as characterized by an unique set of gain and bias, i.e., independently of the specific point under consideration, we refer to it as a *global* TC. In section 3 it was underlined that in this case it is necessary to remove the non-stationary component in time and space which varies on a scale larger than the observation space (thus working with the anomalies), otherwise the hypothesis of constant mean is not kept. This is necessary for the spatial drift, whereas the seasonal variability can be considered as a random component since our observations span a temporal range larger than the typical annual period.

The results are presented in **Table 1**, where ASCAT/H-SAF estimates scaled using a nominally independent set, i.e., either the NOAA or the porosity maps, are considered, and SMOS is taken as reference. The ERA model presents the smallest error (in the order of 3.3 %)

as a consequence of the lower correlation between the two satellite retrievals, and an error slightly smaller than the entire estimated variability of the true variable (around 3.8 %). SMOS has the worst performances, with errors of about 5.3%, due to the lower correlation with ERA with respect to ASCAT/H-SAF. The latter has an error in the order of 4.7 %, which goes up to 5.2 % when the porosity is used for scaling. Note that the results are expressed into the SMOS reference scale, so that ERA-LAND presents a standard deviation of 3.6 % m^3/m^3 and ASCAT/H-SAF scaled using the porosity up to 7.6 % m^3/m^3, when considering their own scale (i.e., multiplying by their respective gains).

SMOS and ASCAT/H-SAF products were also compared to the NOAA soil moisture product using again TC in its *global* configuration. All the three products, were collocated in time and space, removing the spatial drift, as previously done. The results are reported on **Table 2**; they were obtained by choosing again SMOS as reference for an easy comparison with **Table 1**. The NOAA product has a larger error than the others (around 6%), probably due to its very low spatial resolution. It has also a smaller dynamic range (smaller gain, around 0.55), so that its error standard deviation equals about 3.3 % in its own scale, still larger than the others in this scale. This time SMOS slightly outperforms ASCAT/H-SAF, but it is noticeable that their error standard deviation (in the range 5.3-5.5 %) are larger than the standard deviation of the true variable, which is confirmed to be in the order of 3.8-3.9 %.

Table 1: TC results in the *global* configuration considering ERA-LAND, SMOS and ASCAT/H-SAF, with H-SAF product scaled using either NOAA (H-SAF_NOAA) or the porosity maps (H-SAF_POR), and SMOS taken as the reference. σ is the standard

deviation of the true variable, s and ε denote the gain and the error standard deviation, respectively, of each system (indicated by subscript). The spatial trends were removed, whereas the temporal trends were retained.

	σ % m^3/m^3	***s*ERA** #	***s*H-SAF** #	**εERA** % m^3/m^3	**εH-SAF** % m^3/m^3	**εSMOS** % m^3/m^3
H-SAF_ NOAA	3.82	1.09	0.69	3.30	4.75	5.35
H-SAF_ POR	3.83	1.09	1.47	3.31	5.20	5.33

Table 2: Same as Table 1, but considering NOAA data instead of ERA (that replaces NOAA for the purpose of H-SAF scaling)**.**

	σ % m^3/m^3	***s*NOAA** #	***s*H-SAF** #	**εNOAA** % m^3/m^3	**εH-SAF** % m^3/m^3	**εSMOS** % m^3/m^3
H-SAF_ ERA	3.95	0.55	0.76	6.05	5.68	5.25
H-SAF_ POR	3.86	0.56	1.42	5.81	5.44	5.28

4.1.3 *Investigation surface cover factors*

It is worth to compare the performances of the different systems for different surface categories. We performed this comparison both for the pointwise TC (as in section 4.1.1) and *global* TC (as in section 4.1.2). Table 3 reports the error standard deviations, considering the mean value among all the grid points for the pointwise TC. The presence or absence of forest cover (since dense forests can differently act on the two satellite responses), as well as different surface topography (strong topography, flat and moderate topography, flat areas, as annotated in the SMOS product) were considered.

The pointwise TC predicts much better results since it allows the gains to change from point to point, and the better performances of ERA-LAND are generally confirmed in any condition. The impact of forest cover on SMOS is significant, especially for pointwise TC, much higher than that on ASCAT, though SMOS works at lower frequency; this fact could indicate a greater robustness of the ASCAT empirical algorithm to the land cover when looking at temporal changes. Conversely, in non-forested areas SMOS outperforms ASCAT.

In areas where topography is strong topography ASCAT yields the best results when considering pointwise TC, whereas its performance is the worst according to the *global* TC. This is another evidence that the two approaches are not equivalent and must be considered with care to draw final conclusions. The pointwise TC predicts good ASCAT performances in high topography due to the already mentioned robustness of the empirical algorithm to land cover, if one is more interested in the temporal changes. Conversely, the *global* TC put in evidence the much higher influence of topography on ASCAT radar backscatter, with respect to emissivity measured by SMOS. It shows that topography has a significant impact on ASCAT performances when attempting to retrieve the absolute values of *SMC*.

Table 3: TC results in the pointwise (mean value of error standard deviations in the leftmost columns) and *global* configuration (rightmost columns) considering ERA-LAND, SMOS and ASCAT/H-SAF, with H-SAF product scaled using porosity, and SMOS taken as the reference. The spatial trends were removed, whereas the temporal trends were retained.

	Pointwise TC			**Global TC**		
	$\langle\varepsilon_{SMOS}\rangle$	$\langle\varepsilon_{ASCAT}\rangle$	$\langle\varepsilon_{ERA}\rangle$	ε_{SMOS}	ε_{ASCAT}	ε_{ERA}

	Total	3.75	3.54	3.04	5.33	5.20	3.31
Cover	Forest	5.13	4.15	3.91	5.86	5.25	3.47
	No forest	3.11	3.25	2.63	5.03	5.19	3.27
Topography	Flat	3.72	3.52	2.99	5.29	5.06	3.32
	Flat+moderate	3.75	3.54	3.04	5.33	5.20	3.31
	Strong	3.12	2.98	3.27	5.45	7.93	2.09

4.2 Triple colocation considering in-situ data

The TC analysis was also undertaken in its *global* configuration (i.e., retrieving a unique set of gains and error variances) considering station data instead of LSM ones, i.e., considering ISMN upscaled probes, SMOS and ASCAT/H-SAF. While the spatial trend was systematically removed, the seasonal variability was considered either a random component or a non-stationary component and removed, so that the faster changes of soil moisture around the seasonal trend (i.e., the anomalies) were investigated as well. The additive model was considered for the temporal and spatial variability of the drift, as discussed in section 3.2, using the spatial means depicted in **Figure 1**.

The TC technique was applied to the three datasets with ASCAT/H-SAF scaled in different ways, and SMOS was chosen as reference. The results are shown in **Table 4**. The error is around 5% for all three systems, but it is relevant to note that it is larger than the variability of the true variable (in the order of 4.2 % for the anomalies, or 5% including the seasonal variability). SMOS seems to be more capable to detect the seasonal variability, as its error is smaller when the temporal trend is retained, whereas ASCAT/H-SAF slightly outperforms SMOS when looking at the anomaly, except when scaled using NOAA. Surprisingly, satellite data are characterized by slightly smaller errors (around 5% m^3/m^3) with respect to in situ probes (around 5.5% m^3/m^3), an outcome which is worth to be discussed.

We are not considering single moisture probes, as we upscaled the probe measurements to the resolution of the satellites by averaging the values within satellite field of view. Hence, we are evaluating the capability of the probes to reproduce the “average” soil moisture within an area in the order of 40-50 km rather than the capability of the probes to reproduce the moisture at the exact location they are installed. In some pixels we were able to average a significant number of probes, whereas in other pixels the number of available probes is smaller and the local scale variability concurred to increase the estimated noise of the ground system, which is here evaluated at the large scale of the two satellites. In summary, there is the question about how well in-situ local scale measurements are able to represent a satellite coarser observation, encompassing very different landscape conditions (lake, forest, bare soil, topography, etc.) in the field of view.

Table 4: Results of the TC in its global configuration considering SMOS (the reference), ISMN, and ASCAT/H-SAF. ASCAT/H-SAF is scaled using different minimum and maximum maps, derived from ERA, NOAA, or using the porosity (subscript in the first column). The lower figure in the cells refers to the temporal anomalies (both spatial and temporal trends are removed using the additive model).

	σ % m^3m^{-3}	***s*ISMN** #	***s*H-SAF** #	**εISMN** % m^3m^{-3}	**εH-SAF** % m^3m^{-3}	**εSMOS** % m^3m^{-3}
H-SAF_ERA	5.05 4.26	1.00 0.88	0.89 1.04	5.39 5.79	5.60 4.91	4.92 5.08
H-SAF_NOAA	5.13 4.35	0.98 0.84	0.751 0.87	5.62 6.13	5.64 5.12	4.84 5.00
H-SAF_porosity	4.92 4.10	1.06 0.95	1.56 1.84	4.99 5.26	5.55 4.83	5.05 5.21

5. Conclusions

An in depth and extensive comparison of soil moisture retrievals over the area of interest of the EUMETSAT H-SAF project (Europe and North Africa) was carried out considering the H-SAF SM-OBS-1 and the SMOS L2 products (5.51 processor version), as well as in situ measurements and different land surface model predictions (ERA-LAND and NOAA). The analysis spanned a period of 3 years (2010-2012) and the triple colocation approach was used to evaluate the results of the comparison . This technique was reviewed in detail, showing common aspects and differences among few fundamental papers.

ERA yielded the best performances when the point-wise triple colocation was applied to ERA, SMOS and ASCAT/H-SAF products, with average error standard deviation of 3.04% m^3/m^3, as compared to 3.75% m^3/m^3 of SMOS and 3.54% m^3/m^3 of ASCAT/H-SAF. Note that in this case it was assumed that the system gains can vary from point to point, a condition that can be considered as questionable if one looks at satellites and models as a unique system. A *global* TC analysis was also performed and this represents a novelty with respect to literature works; the spatial drift (non-stationary component of the soil moisture field) was removed for this purpose. ERA exhibited the smallest error (around 3.3% m^3/m^3) that turned out to be less than the variability of the true variable (3.8% m^3/m^3); the satellite products error was in the order of 5.3% m^3/m^3 for SMOS and in the range 4.8-5.2% m^3/m^3 for ASCAT/H-SAF, depending on the way the scaling was performed. Replacing ERA with NOAA, the model performances worsened, with error of about 6% m^3/m^3, and SMOS slightly outperformed ASCAT/H-SAF, both just above 5% m^3/m^3, a figure still to be compared with a true variable standard deviation of 3.9% m^3/m^3.

A *global* TC was accomplished considering also the in situ data from the ISMN network. Also in this case the spatial drifts were removed and different ways to scale the ASCAT/H-SAF saturation degree were considered. Although the results changed according to the scaling approach, SMOS slightly outperformed ASCAT/H-SAF when the seasonal variability is left in place (4.9-5.1% m^3/m^3 as compared 5.5-5.6% m^3/m^3), whereas ASCAT/H-SAF performed better in detecting the temporal anomalies (4.8-5.1% m^3/m^3 as compared to 5-5.2% m^3/m^3). Surprisingly, both seemed to perform better than in-situ data (5-6% m^3/m^3), but this can be related to the ability of local in situ probes to represent the average condition within the satellite field of view. It is noticeable that the errors were generally larger than the variability of the true variable (standard deviation in the range 4.1-5.1% m^3/m^3).

When considering the anomalies with respect to the temporal trend, the in-situ data exhibited even worse results, which indicates that their residual short scale variability, in time and space, was not detected by the satellite products and was therefore interpreted as noise by the TC analysis. This demands for a better way to account for the different spatial resolution of the systems, through a characterization of the representative errors throughout geostatistical techniques, which is foreseen in future studies.

Acknowledgements

This work was accomplished in the frame of the EUMETSAT H-SAF project validation activity managed by the Italian Department of Civil Protection (DPC). We thank DPC for its support and in particular Dr. Silvia Puca. The SMOS data were acquired in the frame of the ESA

Cat. 1 project (N. 9720). The ISMN data are available for free at the website https://ismn.geo.tuwien.ac.at/.

Appendix

Starting from eq. (1), under the premise that we estimate r^2, considering all the possible second order statistics of the measured quantities which can be estimated from the TC data set, namely the three variances σ^2_x, σ^2_y, σ^2_z, and covariances $C_{xy}=\langle(x-\langle x\rangle)(y-\langle y\rangle)\rangle$, $C_{xz}=\langle(x-\langle x\rangle)(z-\langle z\rangle)\rangle$ and $C_{yz}=\langle(y-\langle y\rangle)(z-\langle z\rangle)\rangle$, one can write three equations with three unknowns, that are the two scaling factors s_y and s_z and the true variable variance σ^2. It turns out:

$$s_y = \frac{C_{yz}}{C_{xz}} = \frac{\sigma_y}{\sigma_x}\frac{\rho_{yz}}{\rho_{xz}} \qquad s_z = \frac{C_{yz}}{C_{xy} - \sigma_r^2 C_{yz} / C_{xz}} = \frac{\sigma_x \sigma_z \rho_{yz}}{\sigma_x^2 \rho_{xy} - \sigma_r^2 \rho_{yz} / \rho_{xz}} \tag{A.1}$$

In (A.1), the correlation coefficients among observations, i.e., ρ_{xy}, ρ_{xy}, and ρ_{xy} are introduced. The variance of the random errors affecting the three systems can be expressed as:

$$\begin{aligned}
\varepsilon_x^2 &= \sigma_x^2 - C_{xy} C_{xz} / C_{yz} + \sigma_r^2 \\
\varepsilon_y^2 &= \sigma_y^2\, C_{xz}^2 / C_{yz}^2 - C_{xy} C_{xz} / C_{yz} + \sigma_r^2 \\
\varepsilon_z^2 &= \sigma_z^2 \left(C_{xy} / C_{yz} - \sigma_r^2 / C_{xz} \right)^2 - C_{xy} C_{xz} / C_{yz} + \sigma_r^2
\end{aligned} \tag{A.2}$$

Equations (A.2) are slightly different from the expression proposed by Stoeffelen (1998), since, due to the presence of biases and mean $\langle\ \theta\ \rangle$, the variances and covariances replace the second order statistical moments $\langle x^2\rangle$, $\langle y^2\rangle$, $\langle z^2\rangle$, $\langle xy\rangle$, $\langle xz\rangle$ and $\langle yz\rangle$ considered in that paper.

According to an alternative approach (Dorigo et al., 2010; Scipal et al,. 2008), the constant bias affecting the three systems is removed by introducing new observations scaled to the true variable θ space domain (i.e., $x^{\text{¿}} = x/s_x - b_x$; $y^{\text{¿}} = y/s_y - b_y$; $z^{\text{¿}} = z/s_z - b_z$). Then the calibration constants are evaluated applying a simple rescaling of the measurements into the observation space of the reference dataset. More specifically, the mean and variance of *Y* and *Z* systems are scaled to those of the reference *X*, which is implicitly assumed to have unitary gain and null bias (s_x=1, b_x=0) (Dorigo et al., 2010; Hain et al., 2011):

$$y_{\square}^{\text{¿}} = \langle x \rangle + \left(y - \langle y \rangle \right) \square_x^{\square} / \square_y^{\square} \; z_{\square}^{\text{¿}} = \langle x \rangle + \left(z - \langle z \rangle \right) \square_x^{\square} / \square_z^{\square} \quad \text{(A.3)}$$

It can be easily shown that in this way $s_y=\sigma_y/\sigma_x$ and $s_z=\sigma_z/\sigma_x$ are calculated as in (A.1), but setting the correlation coefficients to one and assuming $\sigma_r^2=0$. Considering that from eq. (2) in the main text the differences among the scaled variable turn out to be equal to the difference among the error terms (e.g., $x - y_{\square}^{\text{¿}} = \delta_x - \delta_y$), by cross multiplying those differences, averaging, and considering the assumption of null correlation between errors of different systems, it is possible to obtain a direct estimate of the error variances as well:

$$\varepsilon_x^2 = \left\langle \left(x - y_{\square}^{\text{¿}} \right) \left(x - z_{\square}^{\text{¿}} \right) \right\rangle$$

$$\varepsilon_y^2 = \left\langle \left(x - y_{\square}^{\text{¿}} \right) \left(z_{\square}^{\text{¿}} - y_{\square}^{\text{¿}} \right) \right\rangle \quad \text{(A.4)}$$

$$\varepsilon_z^2 = \left\langle \left(x - z_{\square}^{\text{¿}} \right) \left(y_{\square}^{\text{¿}} - z_{\square}^{\text{¿}} \right) \right\rangle$$

References

Albergel, C., de Rosnay, P., Gruhier, C., Munoz-Sabater, J., Hasenauer, S., Isaken, L., Kerr, Y., Wagner, W., (2012). Evaluation of remotely sensed and modelled soil moisture products using global ground-based in situ observations. *Remote Sensing Environment*, vol. 118, pp. 215-226

Albergel, C., Rudiger, C., Carrer, D., Calvet, J.-C., Fritz, N., Naeimi, V., Bartalis, Z., Hasenauer, S., (2009). An evaluation of ASCAT surface soil moisture products with in situ observations in Southwestern France., *Hydrol. Earth Syst. Sci.*, vol. 13, pp. 115-124

Anderson, W. B., Zaitchik, B.F., Hain, C. R., Anderson, M. C., Yilmaz, M. T., Mecikalski, J., Shultz, L., (2010). Towards an integrated soil moisture drought monitor for East Africa. *Hydrol. Earth Syst. Sci*., vol.16, pp. 2893-2913.

Balsamo G., C Albergel, A. Beljaars, S Boussetta, E Brun, H Cloke, D Dee, E Dutra, F. Pappenberger, P. de Rosnay, J Muñoz-Sabater, T Stockdale, F. Vitart (2014). ERA-Interim/Land: A global land-surface reanalysis based on ERA-Interim meteorological forcing. *Hydrology and Earth System Sciences*, 2014, in review.

Bartalis, Z., Wagner, W., Naeimi, V., Hasenauer, S., Scipal, K., Bonekamp, H., Figa, J., and Anderson, C., (2007). Initial soil moisture retrievals from the METOP-A advanced Scatterometer (ASCAT). *Geophys. Res. Lett.*, 34, L20401, doi:10.1029/2007GL031088.

Brocca, L., Melone, F., Moramarco, T., Morbidelli, R., (2009). Soil moisture temporal stability over experimental areas of Central Italy. *Geoderma*, 148(3-4), 364-374, doi:10.1016/j.geoderma.2008.11.004.

Brocca, L., Hasenauer, S., Lacava, T., Melone, F., Moramarco, T., Wagner, W., Dorigo, W., Matgen, P., Martínez-Fernández, J., Llorens, P., Latron, J., Martin, C., Bittelli, M. (2011). Soil moisture estimation through ASCAT and AMSR-E sensors: an intercomparison and validation study across Europe. *Remote Sensing of Environment*, vol. 115, pp. 3390-3408.

Brown, E.M., Escobar, V., Moran, S., Entekhabi, D., O'Neill, P.E., Njoku, E.G., Doorn, B., Entin, J.K., (2013). NASA's Soil Moisture Active Passive (SMAP) Mission and Opportunities for Applications Users. *Bull. Amer. Meteor. Soc.*, vol. 94, pp. 1125–1128, doi: http://dx.doi.org/10.1175/BAMS-D-11-00049.1

Cimini, D., Pierdicca, N., Pichelli, E., Ferretti, R., Mattioli, V., Bonafoni, S., Montopoli, M., Perissin D., (2012). On the accuracy of integrated water vapor observations and the potential for mitigating electromagnetic path delay error in InSAR. *Atmos. Meas. Tech.*, vol. 5, pp. 1015-1030.

De Jeu, R.A.M., Wagner, W., Holmes, T.R.H., Dolman, van de Giesen, N.C., Friesen J. (2008). Global Soil Moisture Patterns Observed by Space Borne Microwave Radiometers and Scatterometers. *Surv. Geophys.*, Vol.29, pp. 399-420, DOI 10.1007/s10712-0089044-0.

Dorigo , W. A., Scipal, K., Parinussa, R.M., Liu, Y.Y., Wagner, W., de Jeu, R. A. M., Naeimi, V., (2010). Error characterisation of global active and passive microwave soil moisture datasets. *Hydrol. Earth Syst. Sci*, vol. 14, pp. 2605-2616.

Dorigo, W. A., W., Wagner, R., Hohensinn, S., Hahn, C., Paulik, A., Xaver, A., Gruber, M., Drusch, S., Mecklenburg, P., van Oevelen, A., Robock, T., Jackson, (2011). The International Soil Moisture Netweork: a data hosting facility for global in situ soil moisture measurements. *Hydrol. Earth Syst. Sci.*, 15, 1675-1698.

Gruhier, C., de Rosnay, P., Hasenauer, S., Holmes, T., de Jeu, R., Kerr, Y. , Mougin, E., Njoku, E., Timouk, F., Wagner, W., and Zribi, M., (2010). Soil moisture active and passive microwave products: intercomparison and evaluation over a Sahelian site. *Hydrol. Earth Syst. Sci*., vol. 14, pp. 141–156.

Hain, C. R., Cow, W.T., Mecikalski, Anderson M.C., Holmes, T., (2011). An intercomparison of available soil moisture estimates from thermal infrared and passive microwave remote sensing and a land surface modelling. *Journal of Geophysical Research*, vol. 116, D15107.

Hornáček M., W. Wagner, D. Sabel, H. L. Truong, P. Snoeij, T. Hahmann, E. Diedrich, and M. Doubková, (2012). Potential for High Resolution Systematic Global Surface Soil Moisture Retrieval via Change Detection Using Sentinel-1. *IEEE Journal of Selected Topics in Applied Earth Observation and Remote Sensing*, Vol. 5, no. 4, pp. 1303-1311.

Kerr, Y., Waldteufel, P., Wigneron, J.-P., Martinuzzi, J.-M., Font, J. and Berger, M., (2001). Soil Moisture retrieval from space: the Soil Moisture and Ocean Salinity (SMOS) mission. *IEEE Trans. Geosci. Remote Sensing*, vol. 39, pp. 1729–1736.

Kerr, Y. H., Waldteufel, P., Richaume, P.,Wigneron, J. P., Ferrazzoli, P., Mahmoodi, A., et al. (2012). The SMOS soil moisture retrieval algorithm. *IEEE Transactions on Geoscience and Remote Sensing*, 50, 1384–1403.

Kidd R.A., (2005). Implementation Plan for a NRT global ASCAT soil moisture product for NWP, Part 4: Discrete Global Grid Systems. NWP SAF (Satellite Application Facility for Numerical Weather Prediction Associate Scientist Mission Report).

Leroux D.J., Kerr, Y.H., Richaume,P., Berchelot, B., (2011). Estimating SMOS error structure using triple collocation. *Geoscience and Remote Sensing Symposium (IGARSS), IEEE International*, pp.24-27, DOI: 10.1109/IGARSS.2011.6048888.

Leroux, D.J., Kerr, Y.H., Al Bitar, A., Bindlish, R., Jackson, T.J., Berthelot B., Portet G., (2013). Comparison between SMOS, VUA, ASCAT, and ECMWF Soil Moisture Products Over Four Watersheds in U.S.. *IEEE Transactions on Geoscience and remote sensing*, in press, DOI: 0.1109/TGRS.2013.2252468

Liu, Y.Y., Parinussa, R. M., Dorigo, W. A., de Jeu, R. A. M., Wagner, W., van Dijk, A. I. J. M., McCabe, M. F., Evans, J. P., (2011). Developing an improved soil moisture dataset by blending passive and active microwave satellite-based retrievals. *Hydrol. Earth Syst. Sci.*, vol. 15, pp.425-436.

Mattia, F., Le Toan, T., Picard, G., Posa, F.I., (2013). Multitemporal C-band radar measurements on wheat fields. *IEEE Trans. Geosci. Rem. Sens.,* Vol. 41, issue 7, pp. 1551-1560, doi:10.1109/TGRS.2003.813531.

Miralles, D.G., De Jeu, R.A.M., Gash J.H., Holmes T.R.H, and Dolman, A.J., (2011). Magnitude and variability of land evaporation and its components at the global scale. *Hydrol. Earth Syst. Sci*., vol. 15, pp. 967-981, doi: 10.5194/hess-15-967-2011.

Naeimi, V., Scipal, K., Bartalis, K., Hasenauer, S., and Wagner, W., (2009). An Improved Soil Moisture Retrieval Algorithm for ERS and METOP Scatterometer Observations. *IEEE Trans. Geosci. Rem. Sens.,* vol 47, pp. 1999-2013.

Panegrossi, G., Ferretti, R., Pulvirenti, L., and Pierdicca, N., (2011). Impact of ASAR soil moisture data on the MM5 precipitation forecast for the Tanaro flood event of April 2009. *Nat. Hazards Earth Syst. Sci*, vol. 11, pp. 3135–3149.

Parinussa, R. M., Holmes, T. R. H., Yilmaz, M. T., Crow, W. T., (2011). The impact of land surface temperature on soil moisture anomaly detection from passive microwave observations. *Hydrol. Earth Syst. Sci.*, vol. 15, pp. 3135-3151.

Paloscia, S., Pettinato, S., Santi, E., Notarnicola, C, Pasolli, L., and Reppucci, A., (2013). Soil moisture mapping using Sentinel-1 images: Algorithm and preliminary validation. *Remote Sens. Environ.*, vol. 134, pp. 234-248.

Parrens, M., Zakharova, E., Lafont, S., Calve, J.-C., Kerr, Y., Wagnar, W., Wigneron,J.-P., (2012). Comparing soil moisture retrievals from SMOS and ASCAT over France. *Hydrol. Earth Syst. Sci.*, vol. 16, pp. 423-440.

Pierdicca, N. Castracane, P., and Pulvirenti, L. (2008). Inversion of Electromagnetic Models for Bare Soil Parameter Estimation from Multifrequency Polarimetric SAR Data. *Sensors*, vol. 8, pp. 8181-8200.

Pierdicca, N., Pulvirenti, L., and Bignami, C., (2010). Soil moisture estimation over vegetated terrains using multitemporal remote sensing data. *Remote Sens. Environ.*, vol. 114, pp. 440-448.

Pierdicca, N., Pulvirenti, L., Bignami, C., and Ticconi, F., (2013). Monitoring Soil Moisture in an Agricultural Test Site Using SAR Data: Design and Test of a Pre-Operational Procedure. *IEEE Journal of Selected Topics in Applied Earth Observation and Remote Sensing*, vol.6, no.3, pp.1199,1210.

Rüdiger, C., Calvet, J.-C., Gruhier, C., Holmes, T.R.H., de Jeu, R.A.M., Wagner, W., (2009). An intercomparison of ERS-Scat and AMSRE soil moisture observations with model simulations over France. *Journal of Hydrometeorology*, 10(2), 431-447.

Scipal, K., Holmes, T., de Jeu, R., Naeim, V., Wagner, W., (2008). A possible solution for the problem of estimating the error structure of global soil moisture data sets. *Geophysical Research Letters*, vol. 35, L24403.

Stoffelen, A., (1998). Toward the true near-surface wind speed: Error modelling and calibration using triple collocation. *J. Geophys. Res.*, 103, 7755–7766, 1998.

Wagner, W., Lemoine, G., and Rott, H., (1999). A method for estimating soil moisture from ERS scatterometer and soil data—Empirical data and model results. *Remote Sens. Environ.*, vol. 70, no. 2, pp. 191–207.

List of Table captions

Table 1: TC results in the *global* configuration considering ERA-LAND, SMOS and ASCAT/H-SAF, with H-SAF product scaled using either NOAA (H-SAF_NOAA) or the porosity maps (H-SAF_POR), and SMOS taken as the reference. σ is the standard deviation of the true variable, *s* and ε denote the gain and the error standard deviation, respectively, of each system (indicated by subscript). The spatial trends were removed, whereas the temporal trends were retained.

Table 2: Same as Table 1, but considering NOAA data instead of ERA (that replaces NOAA for the purpose of H-SAF scaling).

Table 3: TC results in the pointwise (mean value of error standard deviations in the leftmost columns) and *global* configuration (rightmost columns) considering ERA-LAND, SMOS and ASCAT/H-SAF, with H-SAF product scaled using porosity, and SMOS taken as the reference. The spatial trends were removed, whereas the temporal trends were retained.

Table 4: Results of the TC in its global configuration considering SMOS (the reference), ISMN, and ASCAT/H-SAF. ASCAT/H-SAF is scaled using different minimum and maximum maps, derived from ERA, NOAA, or using the porosity (subscript in the first column). The lower figure in the cells refers to the temporal anomalies (both spatial and temporal trends are removed using the additive model).

List of Figure captions

Figure 1: Maps of minimum (left), maximum (central) and mean (right) values of *SMC* derived from ERA (upper row, years 1991-2012), SMOS with processor version 5.51 (middle row, years 2010-2013) and ASCAT product rescaled using the porosity map (bottom row, years 2010-2013).

Figure 2: Number of colocations of SMOS, ASCAT/H-SAF and ERA-LAND estimates in each point of the ISEA4h9 in the considered time frame grid (January 2010 – December 2012). Note that grid points with more than 150 occurrences are about 4% of the total.

Figure 3: Example of ISMN data up-scaling approach. Blue stars are stations associated to both ASCAT and SMOS field of view, the yellow star is associated only to SMOS and the red star only to ASCAT.

Figure 4: Point wise TC analysis results. Upper row: error variances of ERA-LAND (left panel), ASCAT/H-SAF *SD* (middle panel) and SMOS *SMC* (right panel) systems, all reported in the scale of the ERA-LAND product taken as reference. Bottom row: gain of ASCAT/H-SAF *SD* (left panel) and SMOS (right panel).

Figure 5: RGB level slicing depicting what system performs worse (left) and better (right) than the others. Red: ERA-LAND; green: ASCAT/H-SAF; blue: SMOS**.**